Experimental study of a high-gain harmonic-generation free-electron laser in the ultraviolet

Adnan Doyuran,* Louis DiMauro, William Graves,† Richard Heese, Erik D. Johnson, Sam Krinsky, Henrik Loos, James B. Murphy, George Rakowsky, James Rose, Timur Shaftan, Brian Sheehy, Yuzhen Shen, John Skaritka, Xijie Wang, Zilu Wu, and Li Hua Yu

Brookhaven National Laboratory, Upton, New York, USA

(Received 15 December 2003; published 17 May 2004)

Saturation of a high-gain harmonic-generation free-electron laser (HGHG-FEL) at 266 nm has been accomplished at the Brookhaven National Laboratory/Deep Ultra Violet Free Electron Laser Facility (BNL/DUV-FEL) by seeding with an 800 nm Ti:sapphire laser. We describe the diagnostics used to characterize the electron beam and the FEL output. Analytic and simulation calculations of the HGHG output are presented and compared with the experimental data. We also discuss the chirped pulse amplification of a frequency chirped seed by an energy chirped electron beam. The third harmonic at 88 nm accompanying the 266 nm fundamental has been used in an ion pair imaging experiment in chemistry, the first application of the BNL/DUV-FEL.

DOI: 10.1103/PhysRevSTAB.7.050701 PACS numbers: 41.60.Cr

I. INTRODUCTION

There is considerable interest in producing coherent radiation using single-pass FELs from deep UV down to the x-ray regime [1]. In this Letter, we present a detailed experimental investigation of a high-gain harmonic-generation free-electron laser (HGHG-FEL) in the ultraviolet at 266 nm seeded at 800 nm [2]. An earlier proof-of-principle experiment in the infrared was carried out at the Brookhaven National Laboratory Accelerator Test Facility [3] by seeding with a 10.6 μm CO_2 laser and amplifying the second harmonic at 5.3 μm. The operation of a single-pass FEL in the self-amplified spontaneous emission (SASE) mode has been the subject of many recent studies [4–7]. In this case, the radiation starts from shot noise; therefore, the pulse-to-pulse energy fluctuation is large and the light is not temporally coherent. In the HGHG-FEL [3,8,9], the electron beam is seeded by a conventional laser, which results in a stable central wavelength, excellent temporal and spatial coherence, and high pulse energy stability of the output radiation. Stability of the output pulse energy is limited by fluctuations in the accelerator, not the intrinsic shot noise of the electron beam. The central wavelength is set by the seed laser and inherits its stability. Coherence of the seed laser leads to coherence of the HGHG pulse, which can be Fourier transform limited. The output pulse length can be controlled by the seed laser, thus enabling the production of femtosecond pulses short compared with the electron bunch length.

II. OVERVIEW OF THE DUV-FEL FACILITY

The accelerator consists of a 1.6 cell BNL/SLAC/UCLA rf photocathode gun operating at 2856 MHz with a copper cathode, four SLAC-type linac tanks operating at the same frequency, a 4-dipole chicane, two dipole magnets, as well as a number of quadrupole and trim magnets (Fig. 1). The photocathode rf gun is illuminated by a frequency tripled Ti:sapphire laser at 266 nm producing electron bunches with 300 pC charge, 4 ps FWHM bunch length, 4.5 MeV energy, and normalized projected emittance of 4–5 μm (Table I). Usually the accelerator is operated at a repetition rate of 2.5 Hz but it can be operated at a maximum of 10 Hz at the current configuration. The phase of the drive laser can be independently controlled with respect to rf. The first klystron powers the gun and the first two linac tanks. Two mechanical phase shifters are used to adjust the phase of the gun and the second tank with respect to the first tank. A low-level phase shifter changes the phase of all three sections. The first two linac tanks accelerate the electron beam with the second tank off-crest by 25° to introduce an energy chirp. A 4-dipole chicane compresses the bunch to about 1 ps FWHM, the third linac tank is used to remove the remaining energy chirp with additional acceleration, and the fourth tank accelerates the bunch to 177 MeV. The third and the fourth linac tanks are powered by two separate klystrons so that they can be independently powered and phased. The dipole downstream of the linac is used as the spectrometer for the electron beam. Energy, energy spread, slice emittance, and bunch length can be measured after the dipole at the pop-in monitor located at the upstream beam dump [Fig. 1]. The bunch length is measured with the zero-phasing technique [10].

Downstream of the linac, there are three major components for the HGHG experiment, the modulator undulator, the dispersive magnet, and the radiator undulator. The parameters for the modulator and radiator are shown in Tables II and III, respectively. The dispersive section is a 30 cm long chicane, which converts energy modulation to density modulation.

*Corresponding author.Email address: doyuran@bnl.gov
†Current address: MIT Bates Linear Accelerator Center, Middleton, MA.

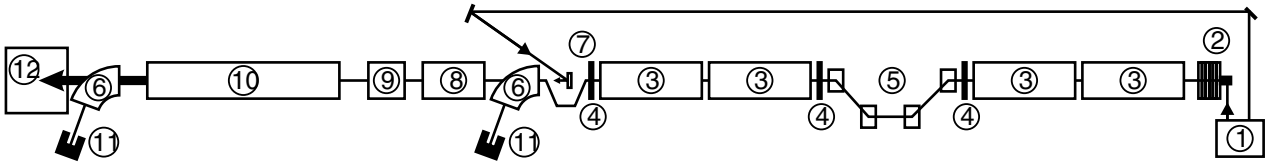

FIG. 1. The National Synchrotron Light Source DUV-FEL layout: 1: gun and seed laser system, 2: rf gun, 3: linac tanks, 4: focusing triplets, 5: magnetic chicane, 6: spectrometer dipoles, 7: seed laser mirror, 8: modulator, 9: dispersive section, 10: radiator (NISUS), 11: beam dumps, 12: FEL measurement area.

The NISUS [11] wiggler (radiator) consists of 16 sections (Fig. 2). Every section is equipped with a pop-in monitor, a four-wire system, and pancake magnets. Pop-in monitors utilizing cerium doped yttrium aluminum garnet crystals are used to monitor the electron beam [12]. The four-wire system at each section can produce quadrupole fields providing additional focusing and a dipole field for trajectory corrections. Pancake shaped magnets located at the top and bottom of the wiggler provide a vertical magnetic field and can be used in a horizontal trajectory correction [13,14]. A fiber coupled He-Ne laser is used for alignment through NISUS. The position of the laser at each monitor is recorded and these positions are used as a reference for the electron beam trajectory. The He-Ne laser is coupled into the beam line by an insertion mirror, which blocks the electron beam. The accuracy of the electron beam position is therefore limited by the reproducibility of the position of the pop-in monitors. On average the pop-in monitors have 30 μm reproducibility, but with optimized mechanical tuning 5 mm reproducibility can be achieved. The position and the beam size of the electron beam at each pop-in monitor are measured and the trajectory of the beam is corrected using automated MATLAB and EPICS routines. This way we also can easily calculate the emittance and the Twiss parameters of the beam and adjust the upstream quadrupole currents to have proper matching into the wiggler (Fig. 3). A number of sections are also equipped with detectors to measure the energy growth along the wiggler. A calibrated Joule meter is used to measure the total energy at the exit. The spectrum of the SASE and HGHG light is measured by a spectrometer with a resolution of 0.025 nm.

TABLE I. Electron beam parameters.

Energy	177 MeV
Charge	300 pC
Normalized projected emittance	4 mm mrad
Normalized sliced emittance	2.5 mm mrad
Uncompressed bunch length	~4 ps (FWHM)
Compressed bunch length	~1 ps (FWHM)
Energy spread	1×10^{-4}

III. ELECTRON BUNCH LENGTH MEASUREMENT USING ZERO-PHASING TECHNIQUE

We use the zero-phasing technique to measure the longitudinal bunch profile. In this method the electron beam is put on the zero degree phase of the tank 4 rf curvature where there is no net energy gain. Because of the almost linear slope, while the head is being accelerated the tail is decelerated or vice versa depending on the sign of the rf slope. This introduces an energy spread that is correlated with the longitudinal position in the bunch. The energy chirp is proportional to the applied field in the accelerator tank. After passing through the upstream dipole magnet, this energy chirp is converted into a horizontal size on the pop-in monitor at the upstream beam dump [Fig. 1]. The longitudinal pulse shape is estimated by measuring the energy of the electron beam and the rf amplitude in the tank. To optimize the resolution of the measurement one has to minimize the horizontal beta function at the monitor using the upstream quadrupoles. Also the energy spread has to be minimized before tank 4.

From the measured energy spectra in Fig. 4, the bunch length is calculated to be 400 fs (rms). The resolution at the spectrometer is optimized by minimizing the betatron beam size. Considering very small intrinsic energy

TABLE II. Modulator wiggler parameters.

Length	0.8 m
Period	8 cm
Peak field	0.22 T
Wiggler parameter (a_{w1})	1.18
Resonant wavelength	800 nm

TABLE III. Radiator wiggler parameters.

Length	10 m
Period	3.89 cm
Peak field	0.31 T
Wiggler parameter (a_{w2})	0.8
Resonant wavelength	266 nm
Betatron wavelength	25 m
Electron beam rms size (4 mm mrad)	250 μm

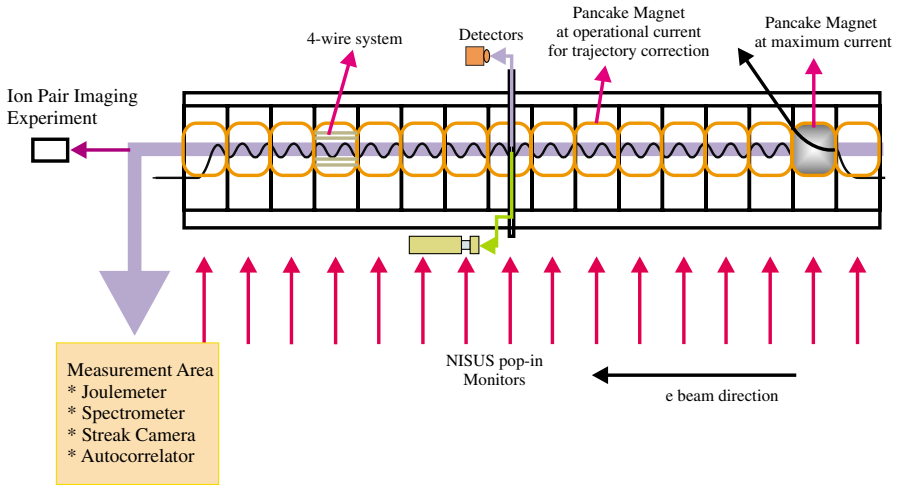

FIG. 2. (Color) 10 m long Nisus wiggler (radiator) and its diagnostics. The four-wire system is used for additional focusing and trajectory correction. The pancake magnet system is used for the horizontal trajectory correction and beam kicking.

spread of the beam, which is about 1×10^{-4}, the resolution at the spectrometer is estimated as 10–20 fs. Clearly, Fig. 4 contains a spiky structure, which, if it results from a modulation of the peak current along the bunch, could degrade the FEL performance. The spikes observed in the measurement are about 100 fs apart. In this case only spikes with high peak current would effectively participate in the FEL process, decreasing output power. Also, since the apparent spike width is comparable to or less than the FEL slippage length, which is 70 μm (230 fs),

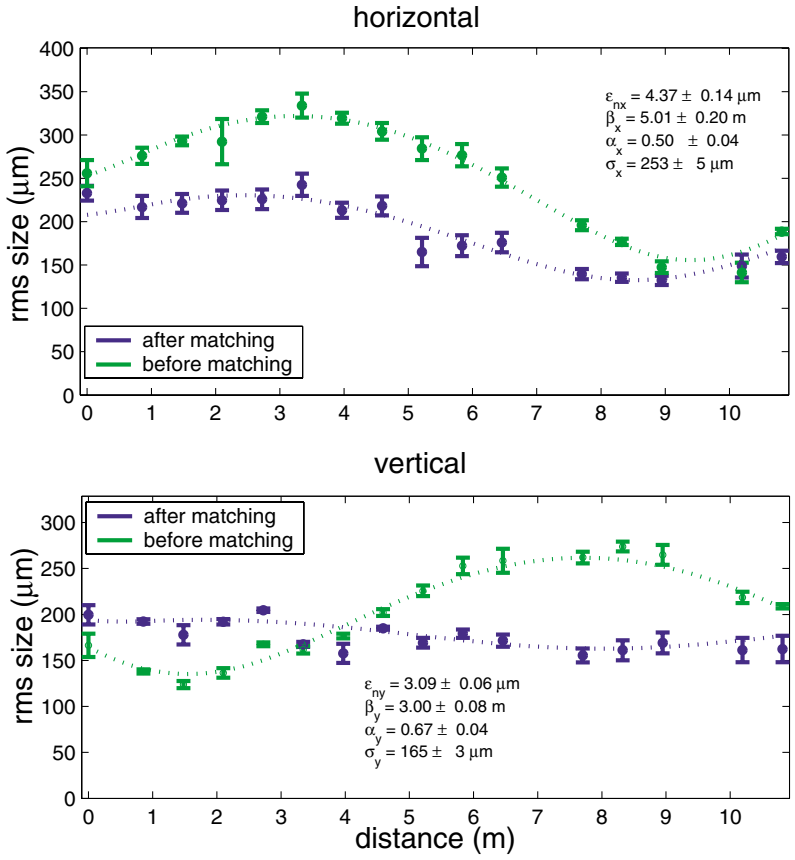

FIG. 3. (Color) Beam matching into the Nisus wiggler using automated MATLAB routines. In figure ε_n is the normalized emittance, α and β are Twiss parameters, and σ is the beam size.

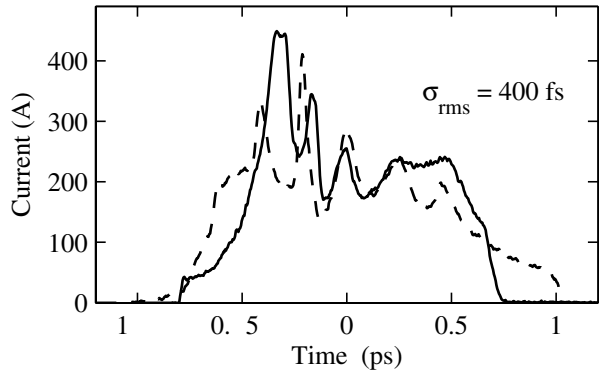

FIG. 4. Current profile measured by zero phasing. The two curves represent two measurements separated by 180. The ripples at the peak are most likely due to small energy modulation; they do not necessarily represent spikes in the time domain [14].

the radiation might not achieve saturation due to slippage between electrons in the spike and radiation in the undulator. In fact, there was no observed degradation of the FEL output observed. This motivated a more detailed inquiry into the proper interpretation of the spiky structure observed on the monitor.

It was shown in Refs. [15,16] that the observed structure results from an energy modulation along the bunch (Fig. 5). Small clusters in electron density, introduced by nonuniformities in the rf gun laser, drive such energy modulation while the beam travels through the accelerator. Since the intrinsic energy spread is small, the energy spectrum of the chirped beam shows a spiky structure

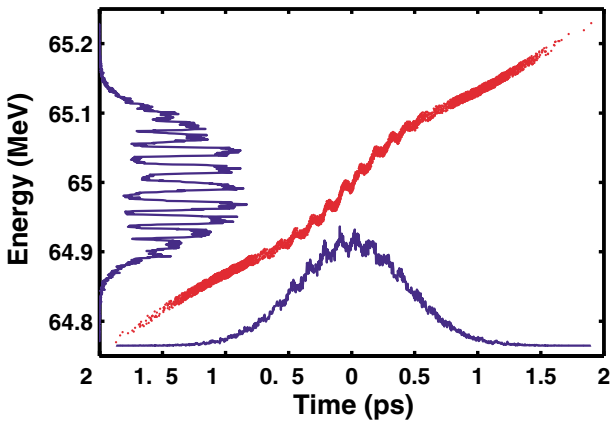

FIG. 5. (Color) Illustration of an electron bunch longitudinal phase space produced by a simulation of a zero-phasing measurement. The horizontal axis is time (ps); the vertical axis is energy (MeV). The space charge wake induces variations of the energy along the chirped bunch leading to deeply modulated energy spectra. The red curve is the distribution of electrons in time-energy phase space. The zero-phasing method measures only the projection on the energy axis whereas there is only a small modulation in the time projection.

resulting from phase space modulation. It was experimentally demonstrated [15] that the observed structure does not represent real bunching in the electron beam longitudinal current.

IV. HGHG PROCESS

The three major components of the experiment are modulator, dispersive magnet, and radiator. The modulator is tuned to the wavelength of the seed laser. The 800 nm seed laser derived from the Ti:sapphire laser with 9 ps FWHM pulse length interacts with the electron beam. A local bump introduced by four trim magnets is used to bypass the seed laser insertion mirror. The Rayleigh range of the seed laser is estimated to be 2.4 m from the beam sizes measured at two pop-in monitor locations in the modulator. Interaction with the seed in the modulator introduces an energy modulation in the electron bunch. The zero-to-peak energy modulation is given by [17]

$$\Delta\gamma = \frac{k_{r1} a_{w1} F_{B1}}{\gamma} a_{r1} z_1. \tag{1}$$

Here γ is the electron beam energy, k_{r1} and a_{r1} are the wave number $(2\pi/\lambda_{r1})$ and the dimensionless (rms) vector potential eA_{r1}/mc of the input laser field, respectively, while a_{w1}, F_{B1}, and z_1 are the dimensionless (rms) vector potential, the Bessel factor, and the length of the modulator, respectively,

$$a_{w1} = \frac{e}{mc} \frac{B_{\rm rms}}{k_{w1}},$$

with

$$k_{w1} = \frac{2\pi}{\lambda_{w1}},$$

$F_{B1} = J_0(\eta) - J_1(\eta)$, with

$$\eta = \frac{a_{w1}^2}{2(1 + a_{w1}^2)}.$$

We estimate $\Delta\gamma \cong 0.5$ for the seed power of 30 MW and $\Delta\gamma \cong 0.1$ for the seed power of 1.8 MW.

When the electron beam passes through the dispersion magnet the energy modulation is converted into a density modulation. We measure the maximum excursion $x_m = 2.1$ mm in the dispersion magnet for a typical current in the coil of 110 A. This corresponds to a dispersion of [9]

$$\left(\frac{d\psi}{d\gamma}\right)_{\rm dis} = 32\pi \frac{x_m^2}{3s\lambda\gamma} \cong 5.4, \tag{2}$$

where λ is the wavelength of the radiator and s is the dispersion magnet length. The radiator [18] is tuned to the 3rd harmonic of the seed laser at 266 nm.

Transverse alignment is established by overlapping the electron and the laser beams on the two pop-in monitors

in the modulator. The synchronization between the electron beam and the seed laser is measured with a picosecond resolution streak camera at the end of the beam line. The SASE and the seed laser pulses are then temporally overlapped by adjusting a delay stage in the seed laser path. The synchronization is further optimized by observing the HGHG output. Varying the dispersion magnet current optimizes the HGHG power. The wiggler is not long enough for SASE FEL to saturate because the typical gain length is about 0.8–1 m and SASE needs more than 20 gain lengths to reach saturation. Since HGHG starts from a prebunched electron beam, the radiation process begins coherently with an effective power large compared with the shot noise and saturates within the length of the wiggler.

The TDA code [9,19] has been utilized to estimate the HGHG power along the wiggler for given initial electron and laser beam conditions. This code is a 3D FEL code which assumes the radiation field to be axially symmetric. It solves numerically the evolution of the Lorentz factor γ and the electron phase $\theta = (k_r + k_w)z - \omega_r t$ coupled with the Maxwell's equations. The code uses the Runge-Kutta method to solve these coupled equations and to find the particle position, momentum, and radiation field, step by step in the z direction.

For HGHG-FEL design purposes we developed a MATHEMATICA program, which calculates the proper input parameters for TDA. We use an analytical estimate developed by Yu *et al.* with scaled parameters [20] and solve Eq. (9) of Ref. [20] numerically which calculates the power gain length of the FEL:

$$Da^2\left[\frac{\mu}{D}\right](1 - e^{-\chi}) - \chi[1 - (1 - \chi)e^{-\chi}] = \int_{-\infty}^{0} \frac{sds}{\cos(\kappa s/D)} \exp\left[-i\left\{\frac{\mu}{D} + \frac{\omega - \omega_r}{\omega_r D}\right\}s - 2\left\{\frac{\sigma_\gamma}{D}\right\}^2 s^2\right] \times \left\{\frac{1 - e^{-\eta_+}}{\eta_+} - \frac{1 - e^{-\eta_-}}{\eta_-}\right\}, \tag{3}$$

with $\chi = -a\sqrt{\mu}H_0^{(1)\prime}(a\sqrt{\mu})/H_0^{(1)}(a\sqrt{\mu})$, and

$$\eta_\pm = 3is\left\{\frac{\kappa}{D}\right\}(k_r\varepsilon) + \frac{\chi}{2}\left[1 \mp \cos\left\{\frac{\kappa}{D}s\right\}\right],$$

$$D = \left[\frac{4eZ_0}{\pi mc^2}\frac{K^2/2}{1 + K^2/2}\frac{I_0}{\gamma_0}\right]^{1/2}[JJ],$$

$$[JJ] = J_0\left(\frac{K^2/2}{2(1 + K^2/2)}\right) - J_1\left(\frac{K^2/2}{2(1 + K^2/2)}\right),$$

$$K = \sqrt{2}a_w = eB_{\text{peak}}/k_w mc \cong 0.934\lambda_w(cm)B_{\text{peak}}(T),$$

$$a = \sqrt{12k_r k_w}\sigma_x, \qquad Z_0 = 377\Omega,$$

$$\kappa = \frac{k_\beta}{k_w}, \qquad k_\beta = \frac{Kk_w}{2\gamma}.$$

Here $k_r = (2\pi/\lambda)$ is the radiation wave number, σ_x is the rms electron beam size, σ_γ is the rms relative energy spread, $k_\beta = (2\pi/\lambda_\beta)$ is the betatron wave number, J_0 and J_1 are the Bessel functions and $H_0^{(1)}$ is the Hankel function.

Equation (3) can be solved to determine the complex parameters χ and $\frac{\mu}{D}$ which yields the power gain length L_G of the FEL as $(1/k_w 2L_G) = \text{Im}(\mu)$. As can be seen from Eq. (3), the gain function can be written in scaled form as [20]

$$G\left(k_r\varepsilon, \frac{\sigma_\gamma}{D}, \frac{k_\beta}{k_w D}, \frac{\omega - \omega_r}{\omega_r D}\right) = \frac{\text{Im}(\mu)}{D} = \frac{1}{k_w 2L_G D}.$$

This is useful to organize parameters for computer simulation codes. Using the MATHEMATICA program, we numerically solve Eq. (3) for a given set of FEL parameters such as emittance, energy spread, and detuning. We start with a scaled detuning of

$$\frac{\omega - \omega_r}{\omega_r D} = -3\left(\frac{k_\beta}{k_w D}\right)k_r\varepsilon$$

which yields near maximum gain as indicated in Ref. [20]. Then the program optimizes the detuning to get the shortest gain length. The typical values for this calculation are shown in Table IV.

The program also calculates the seed laser power and dispersion magnet current for maximum bunching at the beginning of the wiggler [9]. The HGHG power output along the radiator before saturation is

$$P = CP_{\text{coh}}e^{z/L_G}, \tag{4}$$

where P_{coh} is the coherent power at star up and it is proportional to $[\int^{2L_g} \overline{b_n(z, r)}dz]^2$. Here $\overline{b_n(z, r)}$ is the bunching parameter [17] for the nth harmonic averaged over the transverse space. To optimize the initial growth of the HGHG radiation one should maximize the bunching parameter in the first two gain lengths of the radiator. The bunching parameter is

$$b(z, r) = \exp\left[-\frac{1}{2}\left(\frac{d\psi}{d\gamma}(z)\sigma_\gamma\gamma\right)^2\right]J_n\left[n, \frac{d\psi}{d\gamma}(z)\Delta\gamma(r)\right], \tag{5}$$

which is a function of dispersion $d\psi/d\gamma$, local energy spread $\sigma_\gamma\gamma$, and energy modulation $\Delta\gamma$ introduced by the

TABLE IV. Typical FEL parameters from analytical calculation.

D	0.016
k_β	0.264 m^{-1}
k_w	161.5 m^{-1}
k_r	2.36×10^7 m^{-1}
$(\omega - \omega_r)/\omega_r$	-1.57×10^{-3}
L_G	0.75 m

seed laser. The dispersion as a function of distance is [9,17]

$$\frac{d\psi}{d\gamma}(z) = n\frac{k_{w1}}{\gamma}z_1 + \left(\frac{d\psi}{d\gamma}\right)_{\rm dis} + \frac{2k_{w2}}{\gamma}z, \qquad (6)$$

where the first term comes from the modulator, the second term [Eq. (2)] from the dispersive section, and the last term from the radiator. We should note that Eq. (6) is valid only in the first two gain lengths of the radiator before exponential growth. At the end the program produces an input file for the TDA code. This procedure is very efficient, since it does not require iterating parameters in TDA. In a single run we can obtain the HGHG output power as a function of distance.

In Fig. 6 we plot the calculated bunching parameter as a function of distance within the first two gain lengths of the radiator. We obtain maximum bunching when the seed laser power is 30 MW and the dispersion magnet current is 140 A, which corresponds to $(d\psi/d\gamma)_{\rm dis} = 8.7$. Similarly for the seed power of 1.8 MW we obtain maximum bunching at 235 A dispersion magnet current, which corresponds to $(d\psi/d\gamma)_{\rm dis} = 24.9$. However, these cases cause rapid saturation and the total output is reduced due to oversaturation. Therefore, we adjust the dispersion magnet current to optimize the output at the end of the wiggler. Because of a limitation in the dispersion magnet current of 200 A, we cannot reach maximum bunching in the 1.8 MW case. Figure 6 also shows the bunching parameters for 30 MW seed laser power, $(d\psi/d\gamma)_{\rm dis} = 3.5$ dispersion and for 1.8 MW seed laser power, $(d\psi/d\gamma)_{\rm dis} = 8.7$ dispersion corresponding to the conditions for which we present the experimental data (Table V).

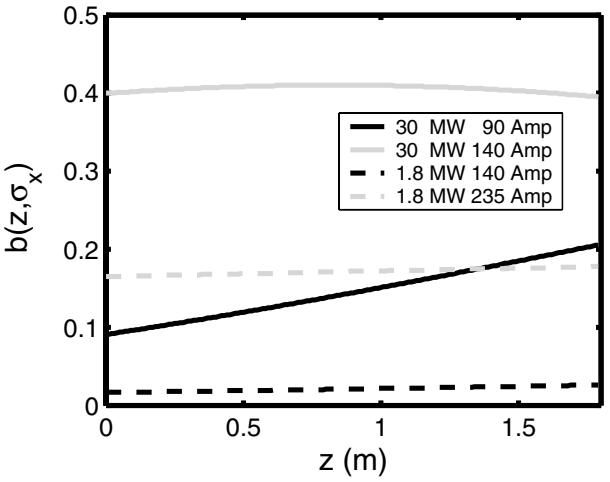

FIG. 6. Calculated bunching factors as a function of the radiator distance within the first two gain lengths using Eq. (4). The solid gray curve is for the maximum bunching where the seed laser power is 30 MW and the dispersion magnet current is 140 A ($d\psi/d\gamma \cong 8.7$); the dashed black curve is for 1.8 MW seed laser power and 140 A dispersion magnet current; the solid black curve is for 30 MW seed laser power and 90 A dispersion magnet current ($d\psi/d\gamma \cong 3.5$); the dashed gray curve is for 1.8 MW seed laser power and 235 A dispersion magnet current ($d\psi/d\gamma \cong 24.9$). Gray curves represent the maximum bunching within the first gain lengths of the radiator, whereas black curves are calculated using parameters actually used during the experiment at each seed power case.

TABLE V. Two experimental cases.

Input seed power	30 MW	1.8 MW
Dispersion	3.5	8.7
Energy modulation	0.5	0.1
Dispersion magnet current	90 A	140 A

V. HGHG OUTPUT MEASUREMENT

We have employed two methods to measure the gain of the FEL. One is measuring the energy using the detectors along NISUS and the other is measuring the energy at the exit Joule meter while kicking the electron beam at different sections using the pancake magnets. Both methods are proven to be consistent with each other.

Figure 7 shows the energy of the HGHG output as a function of the distance in the radiator using the kicking method and simulations of the gain with the TDA code for two input seed powers. We measure the projected emittance of the electron beam as 4.7 mm mrad. For the 1.8 MW case the dispersion section current is set to 140 A, which corresponds to a dispersion $d\psi/d\gamma \cong 8.7$. HGHG saturates near the end of the wiggler. For the 30 MW input seed laser power the dispersion section

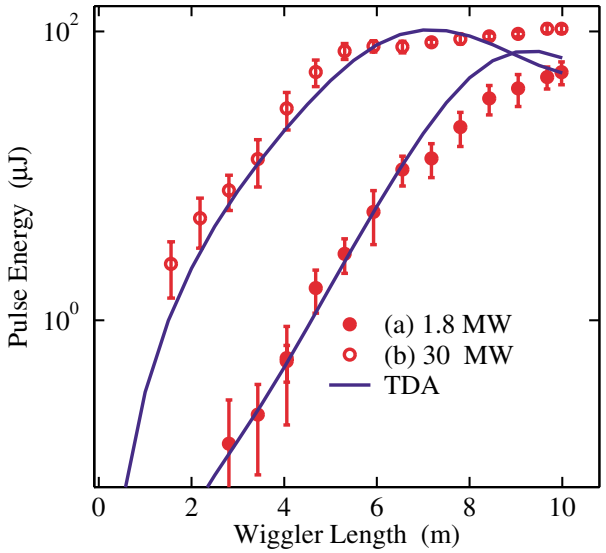

FIG. 7. (Color) Pulse energy vs distance for two values of the input seed laser power: (a) 1.8 MW and (b) 30 MW. The red dots are measurements and the solid curves are TDA simulation results.

current is set to 90 A, which corresponds to dispersion $d\psi/d\gamma \cong 3.5$. HGHG saturates halfway down the wiggler. In each case the dispersion was optimized by measuring the HGHG signal at the end of the wiggler. In the 1.8 MW case, since the dominant contribution to the output comes from the highest current portion of the electron beam, we use the slice emittance of 2.7 mm mrad for the TDA calculation to fit the experimental gain length of about 0.8 m. In the 30 MW case, we approximately take into account the fact that the entire electron bunch contributes by using the projected emittance of 4.7 mm mrad in the simulation to fit the observed experimental gain length, which is about 0.9 m. We see a reasonable agreement between the experiment and the TDA simulation results. We should again note that the dispersion is not optimized for maximum bunching in two gain lengths but it is optimized for maximum total energy at the end of the radiator. In the high seed power case (30 MW) the TDA code predicts that the power should decrease after saturation but the measurement shows the energy still growing very slowly. Since the electron beam has varying current and emittance along the bunch, different parts of the beam reach saturation at different instances resulting in the observed growth in total power after saturation. Figure 8 shows the TDA simulation of energy vs distance for various input seed powers and dispersions. For each case when the dispersion is set to maximum bunching within the first two gain lengths, HGHG saturates rapidly and the output power reduces due to oversaturation. As discussed earlier, in the experiment we set the dispersion to optimize the output at the end of the radiator.

The HGHG output power stability is limited by the accelerator stability but not the intrinsic shot noise in the electron beam. The typical average output is approximately 100 μJ. Figure 9 shows the statistics of the pulse energy measurement. The rms intensity fluctuation is found to be 7% over a half minute. The SASE fluctuation is about 41% for the same electron beam conditions. In the HGHG case the FEL process starts from a nonzero radiation whereas SASE starts from shot noise. Thus the stability of the HGHG output is greatly improved compared to the SASE process. Taking advantage of this stability, the third harmonic at 88 nm, which accompanies the 266 nm, is being used for an ion pair imaging experiment since January 2003 [21]. The typical phase and amplitude instabilities in the various sections of the accelerator cause some small jitters or drifts but these can be solved as accelerator technology improves or by employing feedback systems.

VI. SPECTRUM MEASUREMENT

The spectrum of the FEL output was measured with a high-resolution spectrometer at the end of the beam line. Figure 10 shows the single shot HGHG and SASE spectra. The FWHM bandwidth of the HGHG pulse is 0.23 nm.

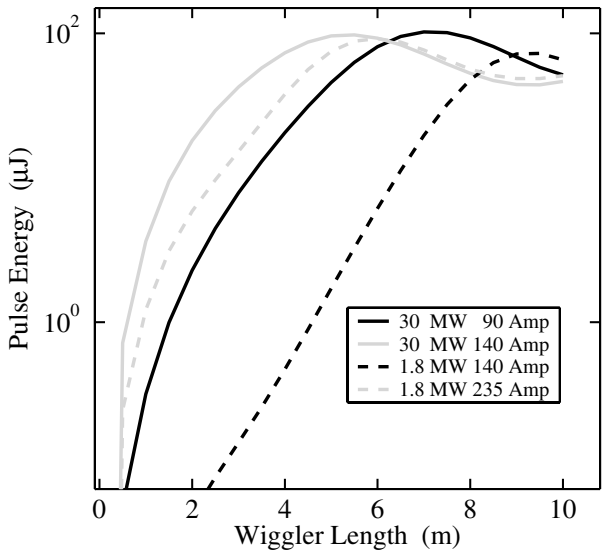

FIG. 8. TDA simulation showing the energy of the HGHG as a function of radiator distance for various seed laser and dispersion magnet currents. For the gray curves the maximum bunching occurs within the first two gain lengths of the radiator, whereas the black curves are simulated using the experimental parameters of each seed power case. The gray curves oversaturate and thus the output power is reduced. For this reason the dispersion is optimized for the maximum output at the end of the wiggler.

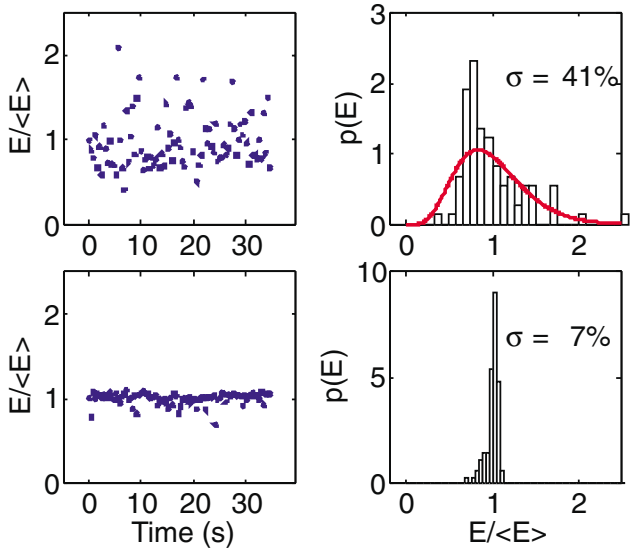

FIG. 9. (Color) Single shot energy measurement of SASE and HGHG for a time interval of 30 s for the same electron beam conditions. Top row is the SASE measurement and the bottom row is the HGHG measurement. The left column shows the actual measurements and the right one shows the histograms of SASE and HGHG output pulse energy with 30 MW seed power. Removing a few data points, which are away from the average due to some machine instability, reduces the σ fluctuation to 3.5%.

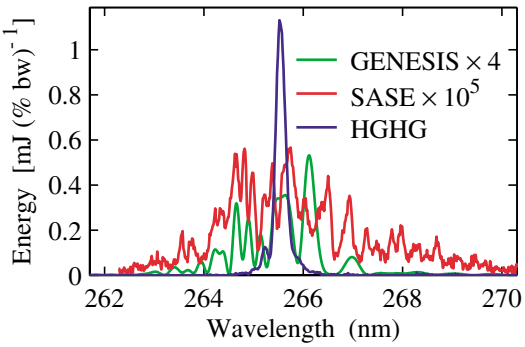

FIG. 10. (Color) Single shot HGHG spectrum for 30 MW seed (blue), single shot SASE spectrum measured by blocking the seed laser (red), and simulation of the SASE spectrum after 20 m of NISUS structure (green). The average spacing between spikes in the SASE spectrum is used to estimate the pulse length.

Since the seed laser is 9 ps long and the electron beam is 1 ps long only 1/9 of the spectrum is seen by the electron beam. The seed laser has ~6 nm bandwidth of which 0.7 nm is interacting with the electron beam. At the third harmonic this corresponds to 0.23 nm bandwidth, which is precisely what was measured. The HGHG spectral brightness is 2×10^5 times larger than SASE because NISUS is not long enough to saturate. To do a fair comparison between SASE and HGHG, we used the GENESIS 1.3 code [22] to calculate what would be the spectrum of SASE after 20 m of the NISUS structure (Fig. 10). Note that due to the larger bandwidth of SASE, HGHG has still an order of magnitude larger spectral brightness than SASE.

VII. PULSE LENGTH MEASUREMENT

The average spacing between the spikes in the SASE spectrum gives an estimate of the radiation pulse length according to [23]

$$T_b = \frac{\lambda^2}{0.64 c \Delta\lambda} = 1 \text{ ps}. \quad (7)$$

The measured electron pulse length (from the zero-phasing method) is 1 ps FWHM which is in good agreement with the above formula.

To measure the HGHG pulse length we used a multishot two-photon absorption (TPA) pump-probe autocorrelator [24] (Fig. 11). A fused silica wedge was used to split the beam into pump and probe. The advantage of using a wedge is that the second reflection beam does not disturb the autocorrelation trace. The transmitted beam serves as the pump and the reflected as the probe. The smaller the ratio of the probe pulse energy to the pump pulse energy, the more sensitive the TPA autocorrelator is. A ratio of 4% was used for convenience of alignment in our case. The pump and probe beams were focused by two plano-convex fused silica lenses with focal lengths of 72 and 31 cm, respectively. The angle between the pump and the probe beam was about 10°. The temporal overlap of the pump and the probe was achieved by manually tuning the micrometer of the delay stage. The resolution of the micrometer is 10 μm. A 5 mm beta barium borate crystal was used for the measurement. The error caused by the thickness of the crystal was about 5 fs, which could be neglected. As shown in the layout of Fig. 11, one photon detector was used to measure the reference signal and another detector was used to measure the transmitted probe pulse signal. By analyzing the ratio of the probe signal to the reference signal vs the delay, one can get the TPA autocorrelation trace.

Assuming the HGHG pulse shape was a Gaussian one, the autocorrelation data were fitted with the least-square method by using the following function:

$$A(t) = C_0 \exp\left[-2\ln 2\left(\frac{t - t_{\max}}{\tau}\right)^2\right] + C_1 t + C_2, \quad (8)$$

where τ is the FWHM pulse length of the HGHG pulse

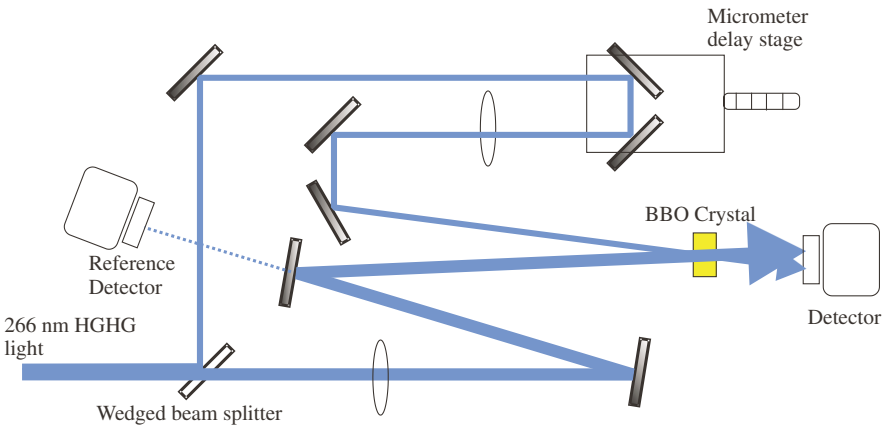

FIG. 11. (Color) The layout of the two-photon absorption pump-probe autocorrelator.

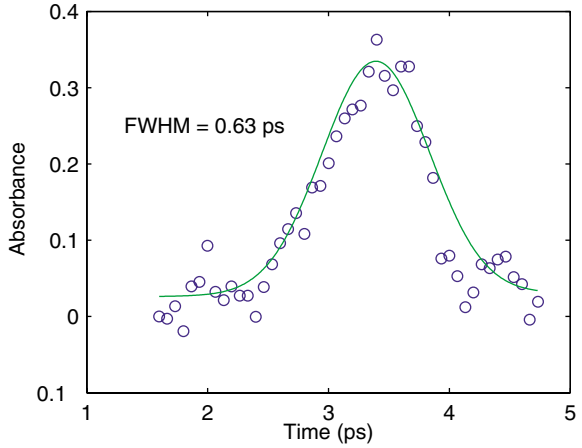

FIG. 12. (Color) Pulse length measurement of the HGHG output using two-photon absorption pump-probe autocorrelation for a seed power of 1.8 MW.

and t_{max} is the time when pump and probe pulses are fully overlapped. The linear part accounts for a drift in the pump.

To reduce the jitter in the measurement signal introduced by fluctuations in the HGHG pulse energy, we used an energy window to reject outliers from the averaging process. We obtained 0.63 and 0.8 ps FWHM (Figs. 12 and 13) for the 1.8 and 30 MW input seed laser cases, respectively.

For the 1.8 MW case, we expect that the pulse shape is close to Gaussian with a slight flattop due to saturation. In the 30 MW case, the pulse should be more like a square shape due to oversaturation. The Fourier transform limited time-bandwidth product depends on the pulse shape. For a Gaussian Fourier transform limited pulse having the measured FWHM bandwidth of 0.23 nm, the FWHM pulse length is $\tau = 0.44$ ps, while for a square Fourier transform limited pulse, the FWHM pulse length is $\tau \cong 1$ ps. The measured pulse length of 0.63 ps for the 1.8 MW seed power is larger than for the Gaussian Fourier transform limited case. This means either the pulse is not fully Fourier transform limited or its peak is flatter than the Gaussian. For the 30 MW seed power, the measured length of 0.81 ps is closer to that of a square Fourier transform limited pulse. As we see in Fig. 7, HGHG reaches saturation in the middle of the wiggler and then the energy grows slowly until the end of the wiggler, indicating that the high current part of the electron beam reaches saturation in the middle of the wiggler, while the lower current parts of the electron beam reach saturation farther down the wiggler and continue to contribute to the total energy. This early saturation of the center and later saturation of the wings suggest the pulse shape should be quite flat.

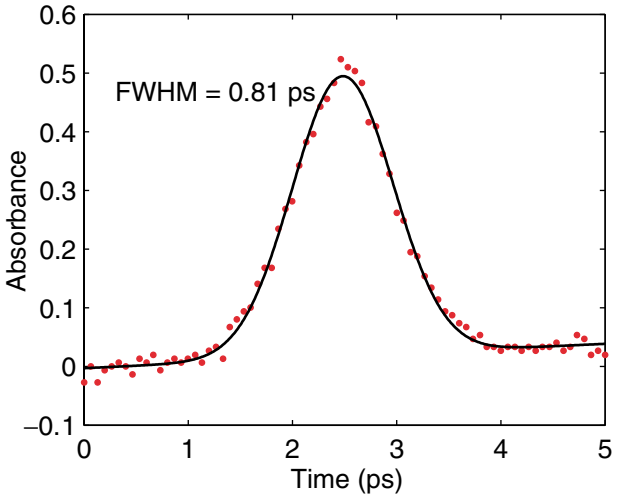

FIG. 13. (Color) Pulse length measurement of the HGHG output using two-photon absorption pump-probe autocorrelation for a seed power of 30 MW.

VIII. AMPLIFICATION OF A FREQUENCY CHIRPED SEED BY AN ENERGY CHIRPED ELECTRON BEAM

There are significant efforts in producing lasers with a pulse length in the femtosecond region. Usually, the photocathode electron guns driving a FEL produce 4–5 ps electron bunches. These bunches can be compressed to 0.1–1 ps; however, it is not trivial to compress electron bunches down to a femtosecond level. By inducing a frequency chirp along the HGHG pulse, we can use conventional laser pulse compressors to shorten the optical pulse duration down to the 10 fs level [25].

In this experiment the seed laser pulse length was adjusted to 1 ps FWHM, which is approximately equal to the electron bunch length. The delay is optimized to fully overlap the seed laser pulse with the electron beam. This way the electron bunch sees the full bandwidth of the seed laser. The FEL process does not amplify the full 1% bandwidth of the chirped seed. The resonant condition for FEL to radiate is

$$\lambda = \frac{\lambda_w}{2\gamma^2}(1 + K^2/2), \tag{9}$$

where K is the wiggler parameter and λ_w is the wiggler period. In order to satisfy this condition along the full electron bunch, we need to introduce an energy chirp to the electron bunch so that every slice within the bunch will be in resonant. Equation (9) yields a relation between the wavelength chirp of the seed laser and the energy chirp of the electron as $(\Delta\gamma/\gamma) = -(\Delta\lambda/2\lambda)$. This implies that for full resonance electron energy chirp should be equal to half of the laser wavelength chirp. We calculate the energy chirp of the electron bunch as follows. The energy of the electron beam after the linac tanks is

$$E = E_{T1} + 34\cos(\phi_2) + 52\cos(\phi_3) + A_{\text{Tank4}}\cos(\phi_4), \tag{10}$$

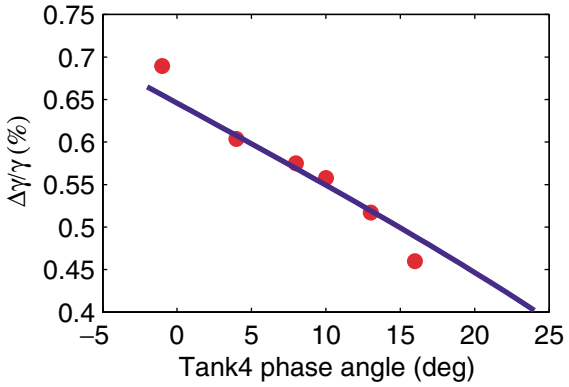

FIG. 14. (Color) FWHM energy chirp of the electron beam as a function of the tank 4 phase. The blue curve is calculated and the red dots are measured.

where E_{T1} is the energy after tank 1 which is fixed during the experiment, A_{Tank4} is the amplitude of tank 4, and each term represents the energy gain at each linac tank in units of MeV; the angles are the tank phases measured with respect to the crest of the rf. The phase of tank 2 is set to $\phi_2 = -22$ to -26 by the compression requirements. Tank 3 is operated on crest ($\phi_3 = 0$), and the tank 4 phase (ϕ_4) is varied to produce different energy chirps in the beam. The amplitude of tank 4 is adjusted so that the total energy is the resonant energy for HGHG-FEL. The energy chirp can be derived by taking the derivative of Eq. (10) and dividing by the total energy

$$\frac{\Delta\gamma}{\gamma} = \frac{\Delta E}{E} = -\frac{34\omega \sin(-22)\Delta t_{\text{uncomp}}}{E} - \frac{A_{\text{Tank4}}\omega \sin(\phi_4)\Delta t_{\text{comp}}}{E}, \quad (11)$$

where ω is the rf frequency, and $\Delta t_{\text{uncomp}} \cong 5$ ps and $\Delta t_{\text{comp}} \cong 1$ ps are the uncompressed and compressed electron bunch lengths, respectively. Figure 14 shows the FWHM percentage energy chirp as a function of the tank 4 phase angle. We observe a good agreement between the measurement and the calculation.

IX. FREQUENCY CHIRPED HGHG SPECTRUM MEASUREMENTS

We scan the phase of tank 4 from 24° to −2° and measure the spectrum in each case. We expect to have the largest bandwidth when the electron energy chirp is half of the seed laser wavelength chirp. Figure 15 shows the spectra for different amounts of chirp. Note that the smoothness of the chirped spectra indicates that the electron density profile is smooth. This is in agreement with the conclusion we reached earlier that the spikes observed in the zero-phasing measurements are due to the induced energy modulation rather than being due to density modulation.

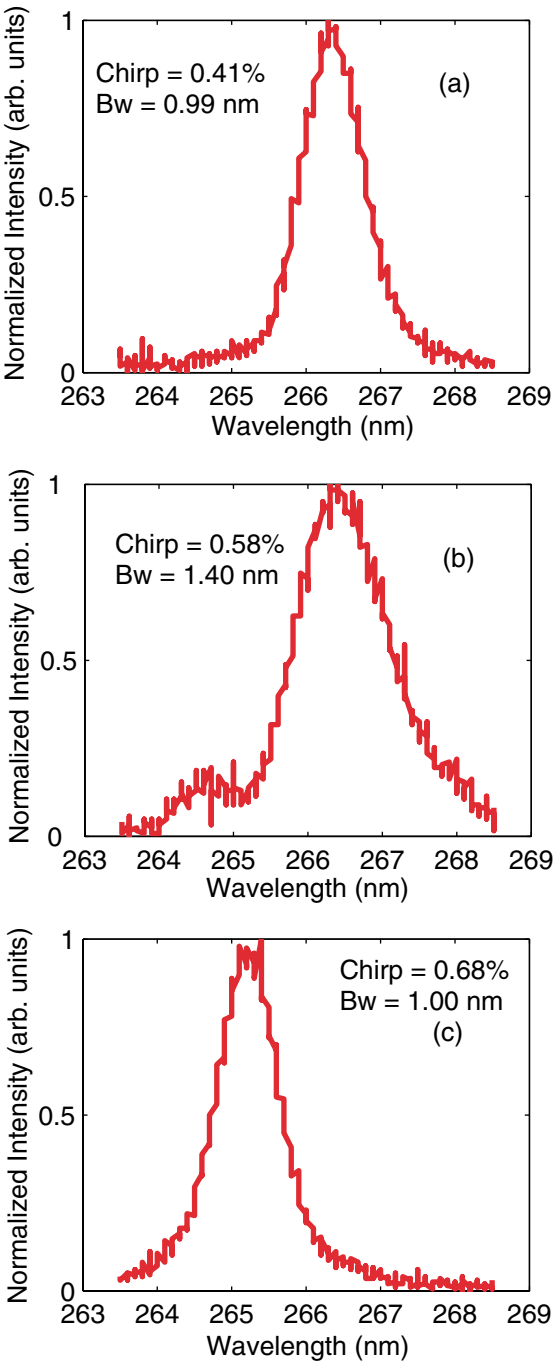

FIG. 15. (Color) (a) Spectrum of CPA-HGHG for a chirp of 0.41%; (b) spectrum of CPA-HGHG for a chirp of 0.58%; (c) spectrum of CPA-HGHG for a chirp of 0.68%

The bandwidth as a function of chirp is shown in Fig. 16. The largest bandwidth is observed when the chirp of the electron beam is matched to the seed laser chirp. We measured the seed laser FWHM bandwidth during the experiment as 5.5 nm, which is about 0.7%. Thus we expect to have the largest radiation bandwidth at 0.35% electron energy chirp and the radiation bandwidth should be 1.8 nm, one-third of the seed bandwidth. The largest

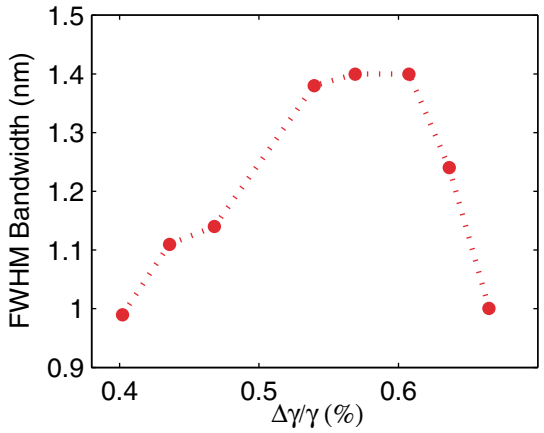

FIG. 16. (Color) HGHG bandwidth vs percent energy chirp of the electron beam. When the electron beam energy chirp is matched to the seed laser frequency chirp we obtain maximum bandwidth.

radiation bandwidth was obtained for an energy chirp of 0.58% rather than the expected value of 0.35%. This may suggest that the electron bunch length is longer than what we measured by the zero-phasing technique [10]. Another possibility is that this is due to the nonlinear energy chirp on the electron beam such as energy modulation due to space charge or rf curvature. At present this is not well understood.

The widest radiation bandwidth achieved was 1.4 nm, not far from the expected value of 1.8 nm. The observed discrepancy may result from the longitudinal jitter of the system since for chirped electron and optical beams the time jitter corresponds to frequency mismatch. We estimate that the time jitter between the electron beam and the seed laser pulse is about 0.15 ps. Considering 1 ps long electron and seed laser beams, 0.15 ps jitter is significant for the performance of the system. The observed intensity and central wavelength fluctuations were larger than in the usual HGHG operational condition. In order to obtain meaningful data in the presence of this jitter, we accumulated a number of spectra for the same electron energy chirp conditions and chose the ones with high output. Currently we are considering a method, which would reduce this jitter by illuminating the cathode with HGHG output at 266 nm. This would reduce the jitter by the compression ratio, which is about 4–5 times.

We are in the process of building a compressor to shorten the CPA-HGHG output and a SPIDER to analyze the output in more detail.

X. CONCLUSION

The DUV-FEL experiment has successfully reached saturation. The output energy is measured to be 100 μJ corresponding to a power more than 100 MW. The output is longitudinally nearly Fourier transform limited and the shot to shot stability is limited by the accelerator performance and not the intrinsic shot noise. The spectral bandwidth is very narrow and as expected and the central wavelength is very stable. We observe a good agreement between the analytic calculations, TDA simulations and experimental data. First steps toward the chirped pulse amplification (CPA) HGHG-FEL have been taken. Spectrum widening has been observed when the electron beam is properly chirped. The results are encouraging for the future compression of the CPA-HGHG output to produce pulses with pulse length in the femtosecond region. A first user experiment at DUV-FEL has started using the 88 nm third harmonic, which accompanies the 266 nm HGHG.

ACKNOWLEDGMENTS

This work was supported by the U.S. Department of Energy, Office of Basic Energy Sciences, under Contract No. DE-AC02-98CH10886 and by the Office of Naval Research Grant No. N00014-97-1-0845.

[1] S. Leone, *Report of the BESAC Panel on Novel Coherent Light Sources* (U.S. Department of Energy, Washington, DC, 1999), http://www.sc.doe.gov/bes/BESCAC/reports.html
[2] L. H. Yu, A. Doyuran, L. DiMauro, W. S. Graves, E. D. Johnson, R. Heese, S. Krinsky, H. Loos, J. B. Murphy, G. Rakowsky, J. Rose, T. Shaftan, B. Sheehy, J. Skaritka, X. J. Wang, and Z. Wu, Phys. Rev. Lett. **91**, 074801 (2003).
[3] Li Hua Yu *et al.*, Science **289**, 932 (2000).
[4] J. Galayda, Linac Coherent Light Source Conceptual Design Report No. SLAC-R-593, 2002.
[5] V. Ayvazyan *et al.*, Phys. Rev. Lett. **88**, 104802 (2002).
[6] S.V. Milton *et al.*, Science **292**, 2037 (2001).
[7] A. Tremaine *et al.*, Phys. Rev. Lett. **88**, 204801 (2002).
[8] I. Ben-Zvi, L. F. Di Mauro, S. Krinsky, M. White, and L. H. Yu, Nucl. Instrum. Methods Phys. Res., Sect. A **304**, 181 (1991).
[9] Li Hua Yu, Phys. Rev. A **44**, 5178 (1991).
[10] D. X. Wang, G. A. Kraft, and C. K. Sinclair, Phys. Rev. E **57**, 2283 (1998).
[11] K. E. Robinson *et al.*, Nucl. Instrum. Methods Phys. Res., Sect. A **291**, 394 (1990).
[12] W. S. Graves, E. D. Johnson, and S. Ulc, in *Beam Instrumentation Workshop*, edited by R. O. Hettel, S. R. Smith, and J. D. Masek, AIP Conf. Proc. No. 451 (AIP, New York, 1998), p. 206.
[13] H. Loos *et al.*, in *Proceedings of the 2002 EPAC, Paris, France* (IEEE, Piscataway, NJ, 2002), p. 837.
[14] H. Loos and T. Shaftan, in *Proceedings of the 2003 PAC Conference, Portland, OR* (IEEE, Piscataway, NJ, 2003), p. MPPB038.
[15] T. Shaftan *et al.*, in *Proceedings of the 2003 PAC Conference, Portland, OR* (Ref. [14]), p. TOPD005; in Proceedings of FEL-2003, Tsukuba, Japan (to be published).

[16] Z. Huang and T. Shaftan, SLAC Report No. SLAC-PUB-9788, 2003; in Proceedings of FEL-2003, Tsukuba, Japan (to be published).
[17] L. H. Yu and J. Wu, Nucl. Instrum. Methods Phys. Res., Sect. A **483**, 493 (2002).
[18] A. Doyuran *et al.*, in *Proceedings of the 2002 EPAC* (Ref. [13]).
[19] T. M. Tran and J. S. Wurtele, Comput. Phys. Commun. **54**, 263 (1989).
[20] L. H. Yu, S. Krinsky, and R. L. Gluckstern, Phys. Rev. Lett. **64**, 3011 (1990).
[21] W. Li *et al.*, Phys. Rev. Lett. (to be published).
[22] S. Reiche, Nucl. Instrum. Methods Phys. Res., Sect. A **429**, 243 (1999).
[23] S. Krinsky and R. L. Gluckstern, Nucl. Instrum. Methods Phys. Res., Sect. A **483**, 57 (2002).
[24] L. I. Isaenko *et al.*, Opt. Commun. **198**, 433 (2001).
[25] L. H. Yu *et al.*, Phys. Rev. E **49**, 4480 (1994).